Energy-based analysis of fatigue–creep interaction in Al–Si/SiC composites at elevated temperature

Krzysztof Wacławiak[a], Goftila G. Sirata[a] and Asfaw Beyene[b]

[a] Department of Materials Technologies, Faculty of Materials Engineering, Silesian University of Technology, Katowice, Poland, Krzysztof.Waclawiak@polsl.pl; goftila.sirata@polsl.pl, CA
[b] Department of Mechanical Engineering, San Diego State University, San Diego, USA, abeyene@sdsu.edu

Abstract:

Structural materials operating at elevated temperatures are often subjected to combined cyclic and time-dependent loading, where fatigue–creep interaction accelerates material degradation and reduces structural reliability. Proper assessment of these interacting effects is essential for reliable material design in high-temperature applications. Aluminum metal matrix composites (AlMMCs) are widely used materials due to their low density, high specific strength, and superior mechanical performance, making them attractive for lightweight applications in the aerospace and automotive industries. Despite these advantages, AlMMCs inevitably undergo long-term degradation under coupled fatigue–creep conditions. This study investigates the sequential fatigue–creep response of an Al–Si/SiC composite under stress-controlled loading at 250 °C. The loading history consisted of repeated fatigue blocks followed by constant-stress creep dwell periods. The evolution of cyclic stress–strain response, ratcheting behavior, maximum strain accumulation, and dissipated strain energy density was experimentally characterized. The experimental results show that their interaction significantly reduces durability and accelerates failure. Combined loading produces complex nonlinear damage and a marked decline in fatigue resistance. Energy dissipation during cyclic loading was also examined, highlighting its contribution to changes in the irreversible microstructural degradation. These findings demonstrate that fatigue dominates the overall energy dissipation, whereas creep contributes indirectly to degradation through its influence on the subsequent cyclic response, indicating that cumulative energy alone cannot fully characterize damage evolution under sequential fatigue–creep loading and that a combined strain–energy framework is required for physically consistent interpretation of Al–Si/SiC composites at elevated temperature.

Keywords:

Aluminum metal matrix composites; Elevated temperature; Energy dissipation; Fatigue–creep interaction; Sequential loading.

1. Introduction

Enhancing the efficiency, reliability, and durability of modern energy systems relies on the continuous development and optimization of advanced engineering materials [1]. Structural components employed in energy-related applications typically operate at elevated temperatures, and they are subjected to complex loading conditions. For instance, components in automotive powertrains [2,3], gas turbine engines [4], steam turbine rotors [5], gas turbine blades [6,7], heat exchangers [8], and aerospace engine components such as compressors [9] regularly experience complex loading histories arising from repeated start-up and shutdown cycles [10,11]. These severe service environments promote progressive microstructural and mechanical degradation, ultimately reducing the component lifetime and structural reliability. Under such conditions, damage evolution is governed by the interaction of multiple mechanisms, particularly cyclic plastic deformation induced by repeated loadings and unloadings. Time-dependent creep deformation, arising from sustained stress at elevated temperatures, becomes imminent. Consequently, high-strength, thermally stable materials are required to endure these interconnected damage processes while preserving long-term structural integrity and functional performance. This creates a need for a reliable product realization process and the characterization of proper materials to ensure the safe, efficient, and reliable operation of energy systems.

Among advanced engineering materials, aluminum metal matrix composites (AlMMCs), particularly those reinforced with silicon carbide (SiC) particles, have emerged as promising alternatives to conventional alloys due to their low density, high specific strength, enhanced thermal stability, and improved resistance to elevated temperatures [12,13]. These properties make them particularly attractive for lightweight structural components in both renewable and conventional energy technologies [14], where reducing structural weight contributes

directly to improved system efficiency and an extended service life [15]. However, unlike monolithic alloys, AlMMCs exhibit a heterogeneous microstructure consisting of a ductile aluminum matrix and stiff ceramic reinforcement, where the size, spatial distribution, and clustering of SiC particles introduce significant local heterogeneities. At the microscale, SiC particles act as barriers to dislocation motion, leading to dislocation pile-up and crack initiation. The mechanical response is governed not only by matrix plasticity but also by matrix–reinforcement load transfer, interfacial integrity, and constraint effects imposed by the particles [16,17].

Under elevated temperature conditions, when materials are subjected to combined fatigue–creep loading, the damage evolution is governed by the interaction between cyclic plasticity and time-dependent creep deformation. This phenomenon, referred to as the fatigue–creep interaction, plays a dominant role in governing material degradation and failure by accelerating damage accumulation. It also results in the nonlinear evolution of the inelastic strain, stiffness degradation, and crack density compared to pure fatigue or creep alone. In AlMMCs reinforced with SiC particles, this interaction becomes more complex due to the microstructural heterogeneity, where the mismatch in thermal expansion between the aluminum matrix and reinforcement generates local residual stresses, and differences in elastic and plastic properties lead to localized strain mismatch [18]. These effects lead to interfacial debonding, particle cracking, and localized stress redistribution, which promote preferential void nucleation sites [19].

At elevated temperatures, the aluminum matrix exhibits viscoplastic behavior in which dislocation rearrangement, dynamic recovery, and grain-boundary sliding accommodate time-dependent deformation, while the matrix–reinforcement load transfer deteriorates through interfacial weakening [20]. This coupled response promotes a transition from matrix-dominated deformation to interface-controlled damage evolution, motivating constitutive frameworks capable of describing localized strain evolution and interfacial degradation.

Two complementary descriptors are commonly used to characterize this coupled phenomenon: strain-based parameters (ratcheting strain, mean-strain shift, cyclic hardening/softening) that track the progressive microstructural state during cyclic loading [21–25], and cyclic energy dissipation, defined as the area enclosed by the stress–strain hysteresis loop, which provides a scalar measure of inelastic work and exhibits a characteristic non-monotonic evolution with damage [26].

Both descriptors are linked to microstructural damage processes such as interface debonding, particle cracking, and void formation, which govern stiffness degradation and the onset of macroscopic failure [27–29]. Experimentally, the interaction is most often probed by (i) cyclic loading with embedded dwell times, which superimposes creep within each cycle, or (ii) sequential loading, in which fatigue and creep are applied in distinct stages and thereby resolves the history dependence of damage accumulation [4,30–32]. While linear damage rules such as Palmgren–Miner [33] cannot capture this nonlinear coupling, more advanced continuum damage models [34,35] remain largely calibrated on monolithic alloys and are rarely validated for heterogeneous AlMMCs. Energy-based interpretations [21,36] face an analogous limitation: under combined loading, dwell-induced time-dependent strain redistributes the cyclic response in ways that cumulative dissipated energy alone cannot resolve.

Although several studies have attempted to address these limitations, important gaps remain in capturing the full evolution of damage under coupled fatigue–creep loading. For example, recent studies have reported that damage evolves gradually during the initial loading stage and accelerates beyond a critical threshold [37], indicating the need for nonlinear-damage models. However, such interpretations often focus primarily on the stabilized and final stages of deformation, with limited attention given to the initial transient response. In practice, material degradation evolves continuously and nonlinearly, beginning with transient strain accumulation during the early loading cycles, followed by a quasi-stabilized regime, and ultimately accelerating toward failure. The early stage is particularly critical because it involves rapid microstructural adjustments and significant nonlinear strain development, which strongly influence subsequent damage evolution. Neglecting this stage may lead to inaccurate life predictions, particularly for components subjected to complex loading conditions. Consequently, a comprehensive nonlinear framework capable of capturing the strain evolution and loading history across all stages of damage, from the initial cycles to the final fracture, is critical.

Two gaps remain. First, existing studies have predominantly focused on monolithic alloys and on stabilized or failure regimes, whereas the early transient stage—where rapid strain accumulation and microstructural rearrangement set the trajectory of subsequent damage—is rarely resolved, particularly under sequential loading in heterogeneous composites. Second, no consistent framework has been proposed that links transient strain evolution to cyclic and dwell-induced energy dissipation in as-cast Al–Si/SiCp composites, where particle clustering and residual stress amplify localized deformation.

In addition, most current approaches treat strain evolution and energy dissipation as separate descriptors, which restricts their ability to capture the coupled and history-dependent nature of fatigue–creep interaction. While energy-based methods provide a useful measure of inelastic work, they do not fully account for the indirect role of creep in modifying the internal material state and subsequent cyclic response. As a result, a unified interpretation linking strain evolution, energy dissipation, and loading sequence across all stages of deformation remains lacking.

Accordingly, this study investigates the isothermal fatigue–creep response of an Al–Si/SiCp composite at 250 °C under sequential stress-controlled loading, comprising repeated fatigue blocks interleaved with creep dwell periods. The objectives are threefold: (i) to resolve the nonlinear strain evolution from the early transient stage to failure and capture it with a stretched-exponential (KWW) saturation law, (ii) to quantify, on a block-by-block basis, the partition of dissipated energy between fatigue and creep segments, and (iii) to demonstrate that cumulative dissipated energy alone cannot describe the interaction, motivating a combined strain–energy interpretation. The present work therefore provides a quantitative basis for evaluating the indirect role of creep in modifying the subsequent cyclic response in particle-reinforced AlMMCs, which is essential for assessing the long-term reliability of lightweight high-temperature components but cannot be resolved using stabilized-regime or pure-fatigue analyses alone.

2. Materials and methods

2.1. Material characterization and experimental procedures

The investigated material was an Al–Si-based aluminum metal matrix composite reinforced with 10 wt. % silicon carbide particles with an average size of approximately 20 μm. Table 1 shows the chemical composition of the alloy matrix, which was determined using optical emission spectroscopy (OES). The composite was fabricated using the stir casting method. Detailed descriptions of the fabrication procedure and processing conditions are provided in the authors' previous work [12].

Microstructural characterization was conducted using light microscopy (LM) and scanning electron microscopy (SEM), as illustrated in Figure 1. The microstructure exhibited an overall near-uniform distribution of SiC particles within the aluminum matrix together with localized particle clustering and particle-rich regions. These microstructural heterogeneities introduce spatial variations in the local mechanical response and act as preferential sites for stress concentration, interfacial debonding, and particle cracking under cyclic and sustained loading conditions. Consequently, such regions strongly influence strain localization, damage initiation, and the subsequent evolution of fatigue–creep interaction mechanisms.

Table 1. Chemical composition of the Al–Si matrix alloy (wt.%).

Al	Fe	Si	Cu	Mg	Zn	Mn	Ti	Ni
Balance	0.4	11.4	1.27	1.24	0.18	0.18	0.04	1.48

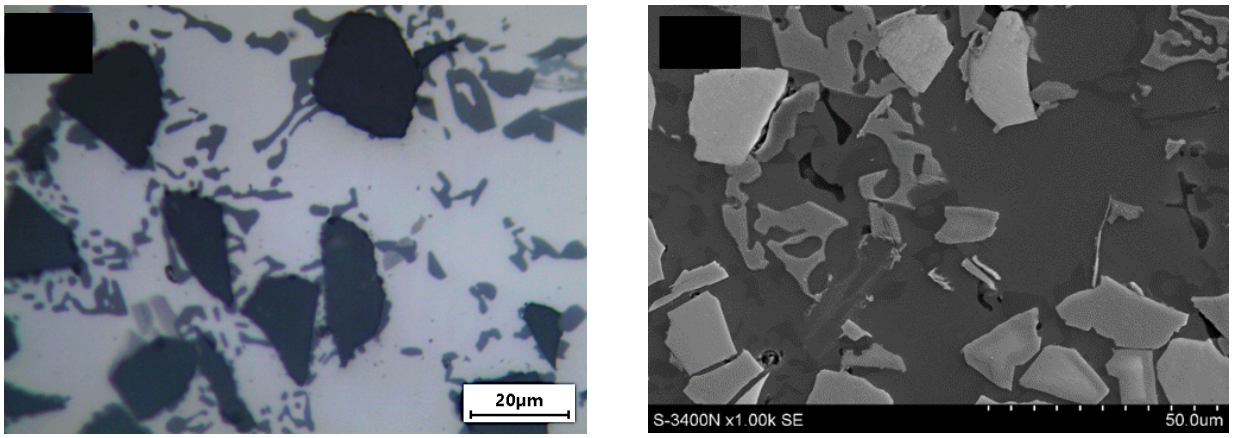

Figure 1. Microstructure of the Al–Si/SiC composite: (a) optical micrograph and (b) SEM micrograph.

Mechanical testing was performed using cylindrical specimens with a gauge length of 60 mm and a diameter of 10 mm. All experiments were conducted using a Zwick/Roell Z100 universal testing machine equipped with a high-temperature resistance furnace. The furnace temperature was maintained at 250 °C with a stability of approximately ±5 °C. Thermocouples attached near the specimen gauge section were used to monitor the specimen temperature during testing. Prior to loading, the specimens were held at the target temperature for 60 min to establish thermal equilibrium and stabilize the specimen surface temperature.

Axial strain measurements were obtained using a high-temperature extensometer with a gauge length of 25 mm attached directly to the specimen gauge section. Load–elongation data were continuously recorded throughout the experiments and subsequently converted into stress–strain responses for analysis of cyclic deformation and strain evolution.

Uniaxial tensile tests were first conducted at 250 °C to determine the elevated-temperature mechanical properties of the investigated composite. The measured ultimate tensile strength (UTS) was approximately 140 MPa. Based on this value, the maximum stress level used during fatigue testing was selected as 50% of the UTS in order to avoid premature failure while maintaining measurable cyclic and time-dependent deformation.

Fatigue tests were performed under uniaxial stress-controlled conditions at 250 °C. The loading parameters were defined as σ_{min} = 7 MPa and σ_{max} = 70 MPa, corresponding to a stress ratio of R = 0.1 (tension–tension loading). A loading frequency of 0.28 Hz was selected to ensure a stable cyclic response and reliable characterization of strain evolution. The chosen stress level represents a regime in which the cyclic plasticity is limited, but the time-dependent deformation effects are active.

All experiments were conducted under isothermal conditions. Throughout the testing, load–elongation data were continuously recorded and subsequently converted into stress–strain responses for analysis of strain evolution and fatigue life. To verify repeatability, five specimens were tested under identical loading conditions. All specimens exhibited consistent overall deformation behavior under the applied fatigue–creep loading conditions, and the reported results represent the typical response of the investigated composite.

2.2. Sequential fatigue–creep loading strategy

To investigate the fatigue–creep interaction, a sequential loading strategy was employed, in which fatigue and creep were applied in distinct stages rather than simultaneously. In this approach, one loading block consists of a fatigue stage, followed by a creep dwell stage. Each fatigue stage was subjected to 10,000 cycles under stress-controlled loading between σ_{min} = 7 MPa and σ_{max} = 70 MPa at a frequency of 0.28 Hz. This was followed by a creep dwell of 10 h at a constant stress equal to σ_{max}. Consequently, the loading sequence can be defined as F → C → F → C → … (until failure), where F denotes the fatigue block and C denotes the creep dwell period.

The duration of each fatigue block was defined by the number of cycles and the cycle period. For 10,000 cycles at 0.28 Hz, where T is the period of one fatigue cycle, the fatigue stage lasted approximately 9.92 h. Including the subsequent 10 h creep dwell, each loading block had a total duration of approximately 19.92 h. Failure occurred after several blocks, allowing for the assessment of the fatigue–creep interaction effects.

The loading history is illustrated in Figure 2 using a stress–time (σ–t) representation. Each block consists of a cyclic stress segment (fatigue) between σ_{min} and σ_{max} and a creep dwell at σ_{max}.

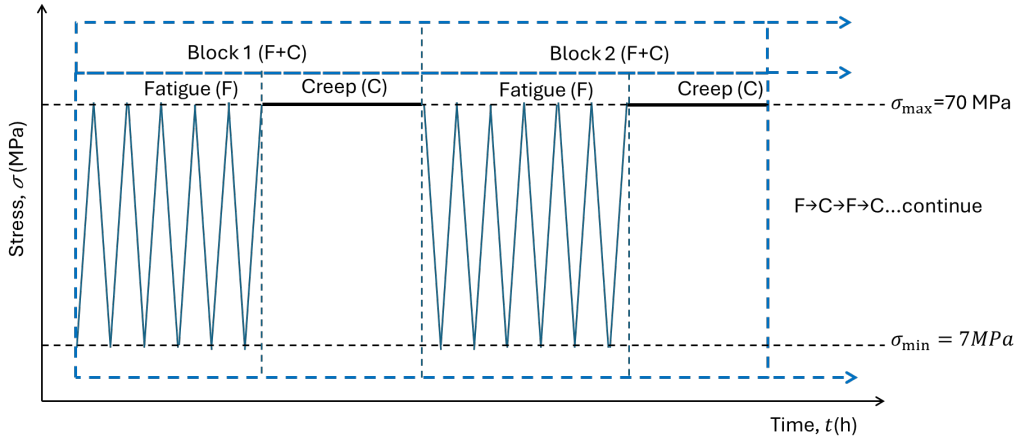

Figure 2. Sequential fatigue–creep loading block.

Each loading block consisted of a fatigue segment followed by a creep dwell. The duration of the fatigue segment, t_f is defined as

$$t_f = N * T, \quad (1)$$

where N is the number of cycles per block and T is the period of one fatigue cycle.

Accordingly, the total duration of one loading block is expressed as

$$t_b = t_f + t_c, \quad (2)$$

where t_c denotes the creep dwell duration.

The starting time of the *k*-th loading block is given by

$$t_k = k * t_b, \quad (3)$$

where k denotes the loading block index (k = 0, 1, 2, …).

Within each block, the applied stress history is defined by Eq. (4):

$$\sigma(t) = \begin{cases} \sigma_{min} + (\sigma_{max} - \sigma_{min})\phi\left(\frac{t - t_k}{T}\right), & t_k \le t < t_k + t_f, \\ \sigma_c, & t_k + t_f \le t < t_k + t_f + t_c, \end{cases} \quad (4)$$

where $\phi(\xi)$ is a normalized periodic waveform defining the stress variation within each fatigue cycle. During the creep dwell, the stress level was maintained at $\sigma_c = \sigma_{max}$.

The function ϕ(ξ) defines the shape of the fatigue cycle as follows: For a triangular waveform, the stress varied linearly during the loading and unloading phases. The normalized periodic function is defined as

$$\phi(\xi) = \begin{cases} 2\eta, & 0 \le \eta < 0.5, \\ 2(1-\eta), & 0.5 \le \eta < 1, \end{cases} \text{ with } \eta = \xi - \quad , \qquad (5)$$

where η represents the fractional part of ξ, ensuring periodicity over each cycle.

During the loading phase ($0 \le \eta < 0.5$), the term 2η produces a linear increase in stress from σ_{min} to σ_{max}. During the unloading phase ($0.5 \le \eta < 1$), the term $2(1-\eta)$ results in a linear decrease back to σ_{min}.

3. Constitutive and energy-based framework

The dissipated strain energy density used in this study provides a direct measure of irreversible deformation during fatigue–creep loading. The energy enclosed within the stress–strain hysteresis loop represents inelastic mechanical work associated with viscoplastic deformation, internal stress redistribution, and progressive microstructural degradation. Consequently, the evolution of dissipated energy offers a direct means of tracking the material state during cyclic and time-dependent loading. Energy-based analysis also provides a link between material-level degradation and the long-term reliability of engineering components that operate at elevated temperatures. Accordingly, the mechanical response under sequential fatigue–creep loading was described using a unified constitutive framework combining cyclic viscoplasticity and time-dependent creep deformation, enabling prediction of the stress–strain evolution during both cyclic loading and dwell periods.

3.1. Cyclic response and creep deformation

The mechanical response under sequential fatigue–creep loading is described using a unified constitutive framework that combines cyclic viscoplasticity and time-dependent creep deformation. This formulation enables the prediction of the stress–strain evolution during cyclic loading and subsequent dwell periods. The cyclic deformation behavior was represented using the Chaboche model, which accounts for both the kinematic and isotropic hardening mechanisms. In the uniaxial form, the stress–strain relationship is expressed as

$$\sigma = E\left(\varepsilon - \varepsilon^p\right), \qquad (6)$$

where σ is the stress, ε is the total strain, E is Young's modulus, and ε^p is the plastic strain.

Plastic yielding is governed by the yield function given by Eq. (7):

$$f = |\sigma - \alpha| - \left(\sigma_y + R\right) \le 0, \qquad (7)$$

where σ_y is the initial yield stress, R is the isotropic hardening variable, α is the total backstress defined as

$$\alpha = \sum_{j=1}^{m} \alpha_j, \qquad (8)$$

Each kinematic hardening component evolves according to the nonlinear Chaboche law expressed by Eq. (9):

$$\dot{\alpha}_j = C_j \dot{\varepsilon}^p - \gamma_j \alpha_j \left|\dot{\varepsilon}^p\right|, \qquad (9)$$

where C_j and γ_j are the material parameters that govern the rate of kinematic hardening and dynamic recovery, respectively. The isotropic response is described using the Voce-type law as follows:

$$R = Q\left(1 - e^{-bp}\right), \qquad (10)$$

where Q and b define the magnitude and rate of cyclic hardening or softening, and p is the accumulated plastic strain.

This framework describes the evolution of the hysteresis loops during cyclic loading, including variations in loop width, shape, mean strain shift, and ratcheting behavior throughout the transient and quasi-stabilized stages. Table 2 presents the calibrated parameters of the combined Voce hardening and Chaboche models at 250 °C. The constitutive parameters were identified using a Python-based nonlinear optimization framework, in which the experimental cyclic stress–strain hysteresis data were iteratively fitted to the predicted constitutive response through least-squares minimization. The optimization simultaneously considered the hysteresis loop shape, stress range, and strain evolution to ensure consistent reproduction of the cyclic response under the applied fatigue loading conditions.

During dwell periods under constant stress, time-dependent creep deformation is initiated. The accumulated creep strain during the dwell of block k is expressed as:

$$\Delta\varepsilon_c^{(k)} = \int_{t_k + t_f}^{t_k + t_f + t_c} \dot{\varepsilon}_c \, dt, \qquad (11)$$

where $\dot{\varepsilon}_c$ is the creep strain rate, and σ_c is the applied dwell stress.

The creep strain rate is described using the Norton power-law relation

$$\dot{\varepsilon}_c = A\sigma_c^n, \quad (12)$$

where A is the temperature-dependent creep coefficient, n is the stress exponent, and σ_c is the applied stress during the dwell period.

Table 2. Constitutive parameters of the composite at 250 °C.

Parameter (Symbol)	*Value*
E (MPa)	65000
Q_∞ (MPa)	-9.5
b	8.5
σ_y (MPa)	45
C_1, γ_1	75000, 1400
C_2, γ_2	45000, 220
C_3, γ_3	7000, 45
A ($s^{-1}.MPa^{-n}$)	1.58×10^{-16}
n	4

The constitutive parameters were identified by fitting the model to the experimental hysteresis loops at selected cycle numbers (50, 100, 500, and 1000 cycles). The optimization minimized the errors in the stress range, loop shape, and maximum strain evolution using a nonlinear least-squares approach. The fitting quality was assessed using RMSE and coefficient of determination (R^2). To determine the creep parameters (A,n), separate creep tests were conducted at 200, 250, and 300 °C under three stress levels (50, 70, and 100 MPa), independently of the sequential fatigue–creep experiments.

3.2. Energy dissipation during sequential fatigue–creep loading

The constitutive response provides the stress–strain history required to evaluate the energy dissipation. The inelastic energy dissipated during the i"-th " fatigue cycle is defined as the area enclosed by the corresponding stress–strain hysteresis loop:

$$W_i = \oint \sigma d\varepsilon, \quad (13)$$

where W_i represents the dissipated energy density during cycle i.

Since the hysteresis loop evolves with cycle number, W_i is generally cycle-dependent and reflects the progressive effects of cyclic plasticity and damage accumulation.

The total energy dissipation during the fatigue stage of block k, containing $N_f^{(b)}$cycles, is obtained by summing the contributions of all cycles.

$$W_k^{(f)} = \sum_{i=1}^{N_f^{(b)}} W_i, \quad (14)$$

where $W_k^{(f)}$ denotes the total fatigue-related energy dissipation within block k.

The main point of the sequential loading condition is that the creep dwell alters the material state between the successive fatigue blocks. As a result, the cyclic response in each subsequent block does not repeat identically. Here, W_i denotes the dissipated energy in the i-th cycle of the considered block.

During the creep dwell, deformation occurs under a constant stress (σ_c). Mechanical work associated with the dwell contributes to dissipation only through the irreversible time-dependent strain component. Therefore, the creep-related dissipated energy during block k is defined by Eq. (15):

$$W_k^{(c)} = \int_{t_k + t_f}^{t_k + t_f + t_c} \sigma_c \dot{\varepsilon}(t) dt, \quad (15)$$

Since σ_c remains constant during the dwell period, Eq. (15) reduces to

$$W_k^{(c)} = \sigma_c \Delta\varepsilon_c^{(k)}, \quad (16)$$

where $\Delta\varepsilon_c^{(k)}$ is the irreversible creep strain accumulated during the dwell period of block k, expressed as

$$\Delta\varepsilon_c^{(k)} = \varepsilon_{c,\,\text{end}}^{(k)} - \varepsilon_{c,\,\text{start}}^{(k)}, \quad (17)$$

where, $\varepsilon_{c,\,\text{start}}^{(k)}$ and $\varepsilon_{c,\,\text{end}}^{(k)}$ denote the creep strain values at the beginning and end of the dwell period, respectively. Here, $\Delta\varepsilon_c^{(k)}$ does not denote the total strain increment during the dwell. It refers only to the time-dependent inelastic creep strain increment after excluding any recoverable elastic contribution. Under the present constant-stress dwell condition, the elastic strain remains approximately unchanged after the stress level is reached; therefore, the measured dwell strain increment was treated as the creep/inelastic strain increment used in Eq. (16).

The total dissipated energy per loading block k is defined as the sum of fatigue and creep contributions as follows:

$$W_k^{tot} = W_k^{(f)} + W_k^{(c)}, \quad (18)$$

where $W_k^{(f)}$ and $W_k^{(c)}$ represent the fatigue and creep contributions, respectively.

The cumulative dissipated energy up to the loading block n is given by

$$W_{cum}(n) = \sum_{k=1}^{n} W_k^{tot}, \quad (19)$$

4. Results and discussion

Below we discuss stress-strain responses, the maximum strain evolution and ratcheting behavior during sequential loading. We will also discuss energy evolution under various conditions including under pure fatigue loading, sequential fatigue–creep loading. Block-wise energy evolution under sequential fatigue–creep loading will also be assessed, with a final statement on impacts of relative contribution of fatigue and creep and energy-based interpretation of fatigue–creep interaction including limitations.

4.1. Cyclic stress–strain response

The applied stress history follows the piecewise definition given in Section 2, where the cyclic loading is represented by a triangular waveform with a constant amplitude and period. The cyclic stress–strain response of the Al–Si/SiC composite at 250 °C is shown in Figure 3, which shows representative hysteresis loops at selected cycle numbers.

The loops remained relatively narrow throughout the loading history, indicating that the material response was predominantly elastic with limited but non-negligible plasticity. Despite their narrow width, a systematic rightward shift in the hysteresis loops was observed with increasing cycle number, indicating the progressive accumulation of inelastic strain. This behavior is characteristic of ratcheting deformation under stress-controlled loading and reflects the sensitivity of the composite to the mean stress and internal stress redistribution.

The early-stage cycles exhibited slightly wider hysteresis loops (e.g., at 50 and 100 cycles), indicating enhanced cyclic plasticity during the transient regime. This response was attributed to the initial accommodation of residual stresses and microstructural heterogeneities in the as-cast composite. As cycling proceeded, the loop width progressively decreased, and a transition toward cyclic stabilization was observed between approximately 500 and 1000 cycles.

This transition reflects the rapid microstructural rearrangement during the early cycles, including dislocation multiplication, localized plastic flow within the Al matrix, and increasing constraints imposed by the SiC particles. At later stages, the cyclic response became more stable, with a reduced plastic strain amplitude. However, the continued shift in the loops indicates that the ratcheting-driven strain accumulation persists even after apparent stabilization. The slight nonlinearity of the loading paths further reflects the heterogeneous deformation behavior arising from the interaction between the ductile matrix and stiff reinforcement.

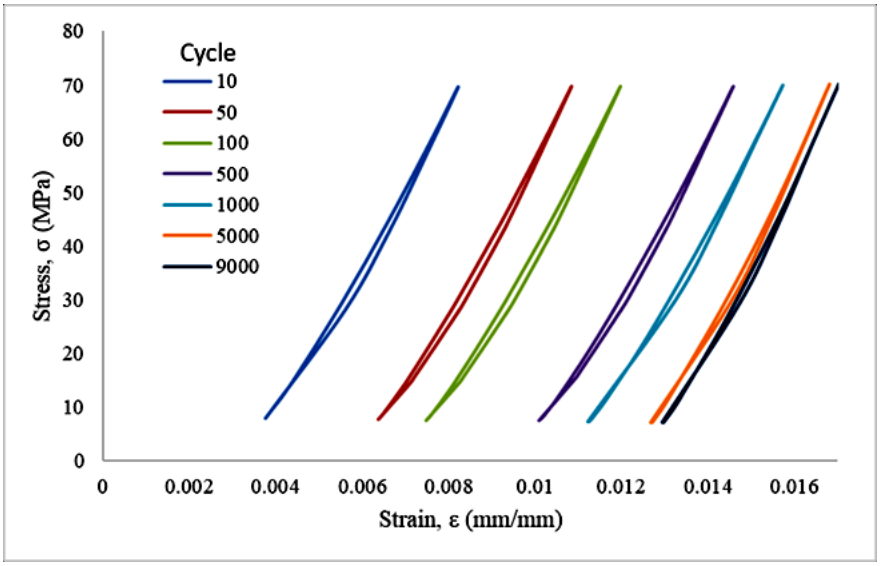

Figure 3. Cyclic stress–strain response of the Al–Si/SiC composite at 250 °C, as shown by the representative hysteresis loops at selected cycle numbers.

4.2. Maximum strain evolution and ratcheting behavior

The evolution of the maximum strain, ε_{max}, with the cycle number is shown in Figure 4. A monotonic increase was observed throughout the loading history, confirming the continuous ratcheting deformation under stress-controlled conditions. The rate of strain accumulation was initially high and gradually decreased with increasing cycle number, indicating a transition from the transient regime to a quasi-stabilized response.

To quantitatively describe this evolution, a stretched exponential function of Kohlrausch–Williams–Watts, (KWW) type, commonly used to describe nonlinear accumulation processes in materials [38], was employed:

$$\varepsilon_{max}(N) = \varepsilon_{\infty} - A\exp\left(-kN^{b}\right), \quad (20)$$

where ε_{∞} represents the asymptotic saturation strain, A is the initial strain offset, and k and b are the rate and curvature of strain accumulation, respectively.

Fitting Eq. (20) to the experimental data yielded the following parameters:

$$\varepsilon_{\infty} = 0.017,\ A = 0.01, k = 0.028,\ b = 0.61$$

The model reproduced the experimental trend with high accuracy ($R^2 \approx 0.99$ and RMSE $\approx 1.62\times10^{-4}$), confirming that the strain evolution follows a nonlinear saturation-type behavior.

This response is consistent with the constitutive equation described in Section 2. The initial rapid increase in ε_{max} corresponds to the transient plastic strain development and rapid evolution of kinematic hardening. With increasing cycles, the rate of evolution decreased, leading to the stabilization of the cyclic response. The asymptotic approach toward ε_{∞} reflects the saturation of both the isotropic and kinematic hardening components. The model predictions show good agreement with both the experimental data and the KWW fit.

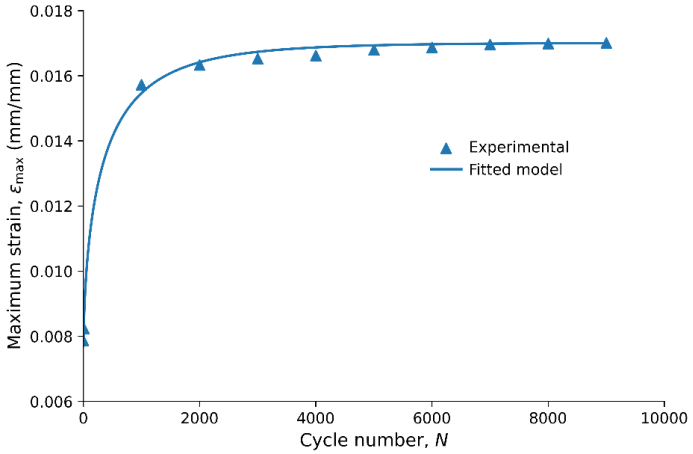

Figure 4. Maximum strain (ε_{max}) as a function of cycle number, including the KWW fit.

4.3. Dissipated energy evolution under pure fatigue loading

The evolution of the dissipated energy per cycle under pure fatigue loading prior to creep exposure is shown in Figure 5. The highest decrease in the dissipated energy was observed during the initial stage of cycling, followed by a gradual transition toward a quasi-stable regime at higher numbers of cycles. Despite minor local fluctuations, the overall trend indicates progressive cyclic stabilization.

The initial reduction in energy was attributed to cyclic accommodation, including the redistribution of internal stress and the reduction in plastic strain amplitude. As the response stabilizes, the rate of energy decrease diminishes, reflecting the reduced cyclic plasticity under stress-controlled loading conditions.

The behavior was fitted using the KWW-type decay function:

$$W(N) = W_S + A\exp\left[-\left(\frac{N}{\tau}\right)^{\beta}\right], \quad (21)$$

With: $W_S = 1.43\times10^{-3}\text{MJ/m}^3, A = 1.02\times10^{-2}\text{MJ/m}^3, \tau = 913.74, \beta = 3$

The model captured the overall trend well ($R^2 = 0.92$), confirming that the energy dissipation decreased as the material approached cyclic stabilization.

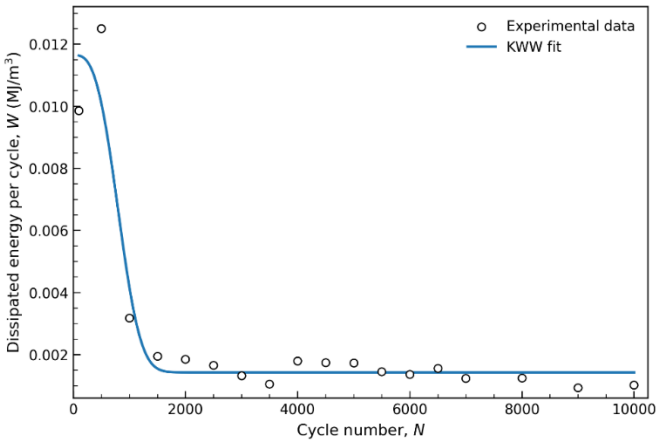

Figure 5. Dissipated energy per cycle during pure fatigue loading with KWW fitting.

4.4. Block-wise energy evolution under sequential fatigue–creep loading

Figure 6 shows the cumulative dissipated energy per fatigue block during the sequential fatigue–creep loading. In contrast to the pure fatigue behavior, the energy evolution is not strictly monotonic but exhibits fluctuations between the successive blocks.

This behavior arises from the influence of intermediate creep dwell periods, which modify the internal state of the material via stress relaxation, deformation, and microstructural rearrangement. Consequently, the cyclic response in each fatigue block reflected both the prior fatigue damage and the creep-induced changes.

A decreasing trend was observed from F1 to F3, indicating progressive cyclic stabilization. However, the increase in F4 suggests a transient reactivation of inelastic deformation, possibly associated with accumulated damage, local stress concentration, or degradation of the particle–matrix interface.

In the final block (F5), a sharp reduction in energy was observed, which was attributed to premature failure after approximately 3000 loading cycles. This is because the reduced energy resulted from the shortened fatigue block.

Creep dwell contributes to additional deformation and alters the internal state governing the subsequent cyclic response. Consequently, the cyclic response in subsequent fatigue blocks reflects the combined effects of prior cyclic damage and time-dependent deformation, leading to non-monotonic energy evolution.

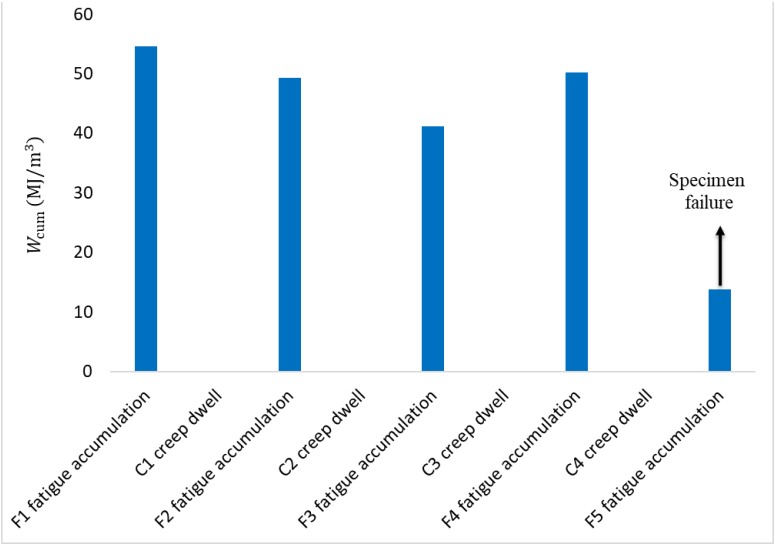

Figure 6. Cumulative dissipated energy per fatigue block during sequential fatigue–creep loading.

4.5. Maximum strain evolution during sequential loading

The segment-wise evolution of the maximum strain, defined as the peak strain recorded within each fatigue and creep segment, is illustrated in Figure 7. The response exhibited a stepwise pattern associated with alternating fatigue and creep segments. The highest maximum strain was observed during the initial fatigue block (F1), which corresponded to the transient accommodation stage. Subsequently, the strain rate decreased and stabilized. Each creep dwell (C1, C2, etc.) resulted in a distinct increase in the maximum strain, whereas the subsequent fatigue blocks exhibited reduced accumulation rates or partial relaxation. This behavior reflects the interaction between cyclic plasticity and time-dependent creep deformation. The observed strain

increments during the creep dwell are consistent with the formulation in Section 2, where the creep strain is defined as the time integral of the creep strain rate. The inset demonstrates that even small strain increments accumulate progressively over successive blocks, confirming a strong dependence on the loading history.

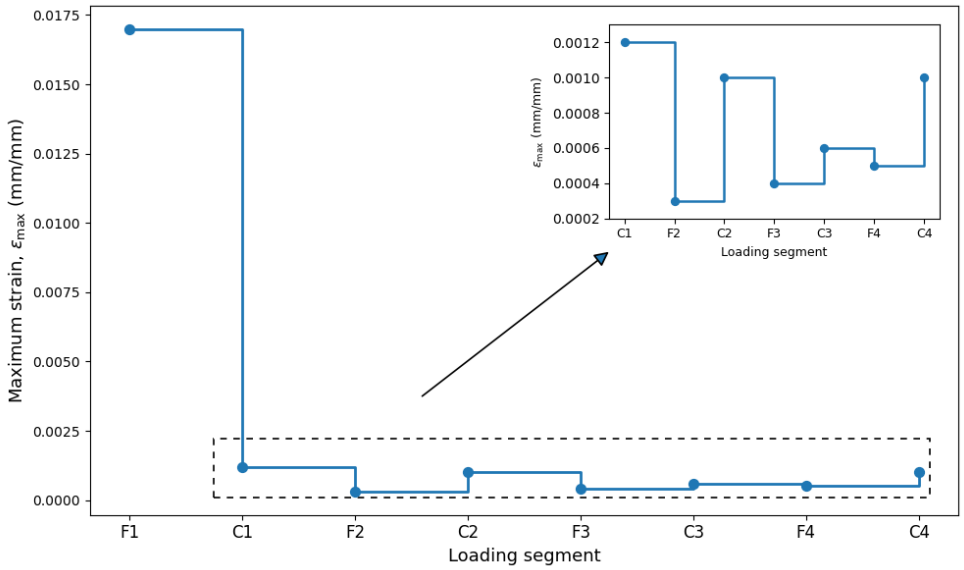

Figure 7. Maximum strain during sequential fatigue–creep loading; inset indicates later loading blocks.

4.6. Cumulative energy dissipation and fatigue–creep interaction

Figure 8 shows the cumulative dissipated energy during sequential fatigue–creep loading. The energy evolution exhibits a stepwise pattern, where the major increments correspond to the fatigue segments and the comparatively small increases correspond to the creep dwell periods.

The fatigue blocks contributed approximately 41–55 MJ/m³ per segment, indicating that cyclic plasticity dominates the overall dissipative response through repeated hysteresis loop accumulation over thousands of cycles. In contrast, the creep dwell periods produced only minor energy increments of approximately 0.05–0.09 MJ/m³ despite measurable strain accumulation during the dwell stages. Under constant stress conditions, creep contributes energy primarily through monotonic time-dependent strain accumulation rather than cyclic hysteresis dissipation.

However, the relatively small energy contribution of creep does not imply a negligible influence on deformation evolution. The creep dwell periods introduce additional strain accumulation and stress redistribution, which modify the subsequent cyclic response and contribute indirectly to progressive microstructural degradation. This effect is reflected in the non-uniform energy increments between successive fatigue blocks and the altered hysteresis behavior observed after each creep interruption. The reduced energy increase during the final fatigue block is associated with premature failure after approximately 3000 cycles.

These observations demonstrate that cumulative dissipated energy alone is insufficient to fully characterize fatigue–creep interaction under sequential loading conditions. Although fatigue dominates the total energy dissipation, creep significantly influences the subsequent cyclic response through modification of the internal material state. Consequently, the block-wise fatigue energy should be interpreted not as an independent measure of damage, but as an indicator of the evolving deformation behavior after each creep dwell period.

Accordingly, the present results are consistent with previous studies on particulate-reinforced Al/SiC composites reported by Barbera et al. [18], Llorca [19], Prasad et al. [30], and Giuliano et al. [23], which also identified progressive strain accumulation, cyclic softening–stabilization behavior, and creep-assisted degradation under elevated-temperature loading conditions. However, the present study further demonstrates that, under sequential fatigue–creep loading, the direct creep-related energy contribution remains comparatively small relative to the fatigue hysteresis dissipation, despite its significant influence on subsequent cyclic deformation and ratcheting evolution. The obtained saturation strain behavior and nonlinear strain accumulation described by the KWW model additionally support the interpretation that creep–fatigue interaction cannot be fully characterized using cumulative energy dissipation alone. Therefore, a combined assessment of strain evolution and energy partition provides a more physically consistent interpretation of fatigue–creep interaction in Al–Si/SiC composites operating under elevated-temperature service conditions.

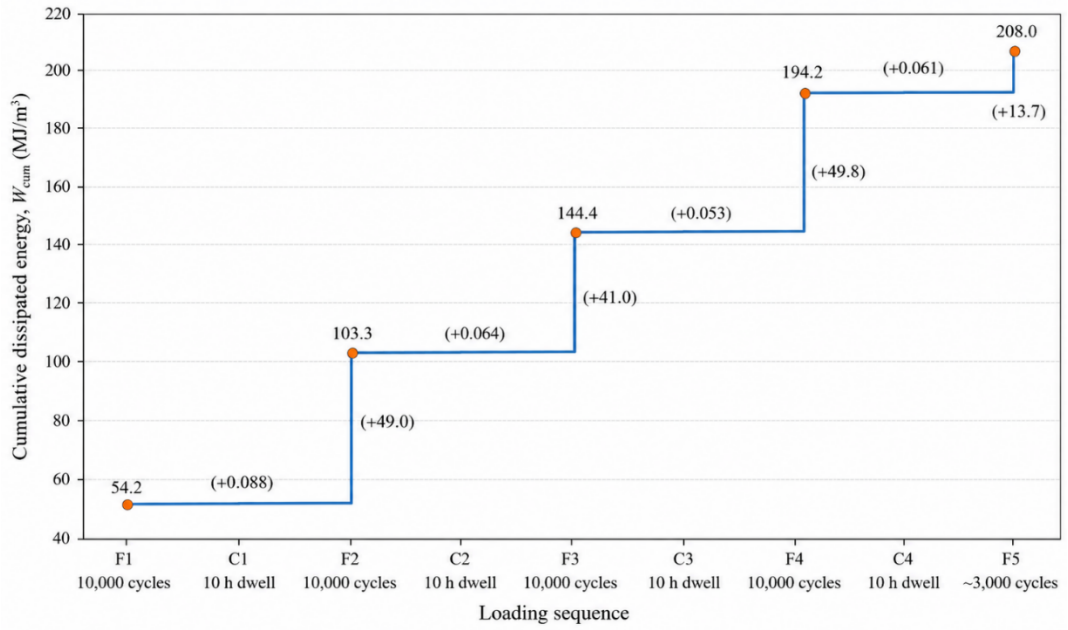

Figure 8. Cumulative dissipated energy during sequential fatigue–creep loading.

Conclusions

The fatigue–creep interaction behavior of the investigated Al–Si/SiC composite at 250 °C was investigated under stress-controlled loading by analyzing the cyclic stress–strain response, strain evolution, and energy dissipation behavior. The material response was dominated by elastic deformation with limited cyclic plasticity, yet exhibited clear ratcheting behavior characterized by progressive hysteresis-loop shift and continuous accumulation of inelastic strain. The evolution of the maximum strain followed a nonlinear saturation trend that was successfully described using a stretched exponential KWW model with a saturation strain of ε_{∞} = 0.017, indicating a transition from transient cyclic deformation toward a quasi-stabilized response.

Under pure fatigue loading, the dissipated energy per cycle decreased rapidly during the initial stage and gradually approached a quasi-stable regime, indicating cyclic accommodation and a reduction in the plastic strain amplitude. In contrast, sequential fatigue–creep loading introduces a pronounced history dependence. Creep dwell periods lead to additional inelastic strain and significantly alter the subsequent cyclic response, resulting in stepwise strain evolution and non-monotonic variations in block-wise energy dissipation. Failure under sequential loading occurred after approximately four complete loading blocks and partial completion of the fifth block, corresponding to substantially reduced fatigue endurance relative to pure fatigue loading.

The fatigue segments contributed approximately 41–55 MJ/m³ of dissipated energy per block, whereas the creep dwell periods contributed only about 0.05–0.09 MJ/m³ despite measurable time-dependent strain accumulation. These results indicate that fatigue dominates the overall energy dissipation, whereas creep contributes indirectly to degradation through progressive strain accumulation and internal stress redistribution that alter the subsequent cyclic response.

The present results demonstrate that fatigue–creep interaction in Al–Si/SiC composites cannot be fully interpreted using dissipated energy alone. Although fatigue dominates the total energy dissipation, creep significantly alters the subsequent cyclic response through strain accumulation and internal stress redistribution. Consequently, a coupled strain–energy framework is required to describe the evolution of deformation and degradation under elevated-temperature sequential loading conditions. The proposed approach therefore provides a consistent framework for assessing long-term reliability and deformation-driven degradation in lightweight materials intended for elevated-temperature engineering applications.

References

[1] Simões S., Advances in the design and development of lightweight metal matrix composites: processing, properties, and applications. Metals 2025;15:1281. https://doi.org/10.3390/met15121281.

[2] Valsan A., Evaluation of mechanical properties of reduced stress localized aluminium composites for automobile applications. In: 11th SAEINDIA International Mobility Conference (SIIMC 2024); 2024 Dec 11; New Delhi, India. SAE Technical Paper 2024-28-0241. https://doi.org/10.4271/2024-28-0241.

[3] Lattanzi L., Mohammadpour Kasehgari S., Awe SA., The influence of SiC particle reinforcement on the thermophysical properties of aluminium-based metal matrix composites. J Therm Anal Calorim 2025;150:10855-66. https://doi.org/10.1007/s10973-025-14475-3.

[4] Gorgannejad S., Estrada Rodas EA., Neu RW., Employing sequential experiments to gain insights on the interaction between creep and fatigue damage in Ni-base superalloys. Fatigue Fract Eng Mater Struct 2022;45:1981-94. https://doi.org/10.1111/ffe.13715.

[5] Holdsworth SR., Mazza E., Binda L., Ripamonti L., Development of thermal fatigue damage in 1CrMoV rotor steel. Nucl Eng Des 2007;237:2292-301.

[6] Segersäll M., On thermomechanical fatigue of single-crystal superalloys [dissertation]. Linköping, Sweden: Linköpings Universitet; 2014.

[7] Norman V., Stekovic S., Jones J., Whittaker M., Grant B., On the mechanistic difference between in-phase and out-of-phase thermo-mechanical fatigue crack growth. Int J Fatigue 2020;135:105528.

[8] Lee H-Y., Lee Y-B., Kim J-B., Evaluation of creep-fatigue damage for heat exchangers in the Stella sodium test loop. Procedia Eng 2013;55:326-32. https://doi.org/10.1016/j.proeng.2013.03.261.

[9] Sun D., Ma G., Wan Z., Gao J., Study on creep-fatigue interaction mechanism and life prediction of aero-engine turbine blade. Eng Fail Anal 2023;154:107715. https://doi.org/10.1016/j.engfailanal.2023.107715.

[10] Viswanathan R., Damage mechanisms and life assessment of high temperature components. Materials Park, OH, USA: ASM International; 1989.

[11] Wang R-Z., Zhang X-C., Tu S-T., Zhu S-P., Zhang C-C., A modified strain energy density exhaustion model for creep-fatigue life prediction. Int J Fatigue 2016;90:12-22. https://doi.org/10.1016/j.ijfatigue.2016.03.005.

[12] Sirata GG., Wacławiak K., Dolata AJ., Microstructure and mechanical properties of the EN AC-AlSi12CuNiMg alloy and AlSi composite reinforced with SiC particles. Arch Foundry Eng 2024;24(2):50-59.

[13] Gopalakrishnan T., Pugazhenthi R., Kanan M., Tank G., Simon D., Effects of thermal shock on mechanical properties and microstructural integrity of aluminum-SiC composites. AIP Adv 2025;15(11):115111. https://doi.org/10.1063/5.0282917.

[14] Wąsik A., Leszczyńska-Madej B., Madej M., Sustainability in the manufacturing of eco-friendly aluminum matrix composite materials. Sustainability 2024;16:903.

[15] Rey P., González-Doncel G., Advances in lightweight metal matrix composites. Metals 2025;15:160.

[16] Alem SAA., Sabzvand MH., Govahi P., Poormehrabi P., Hasanzadeh Azar M., Salehi Siouki S., et al., Advancing the next generation of high-performance metal matrix composites through metal particle reinforcement. Adv Compos Hybrid Mater 2025;8:3. https://doi.org/10.1007/s42114-024-01057-4.

[17] Su Y., Ouyang Q., Zhang W., Li Z., Guo Q., Fan G., Zhang D., Composite structure modeling and mechanical behavior of particle reinforced metal matrix composites. Mater Sci Eng A 2014;597:359-69. https://doi.org/10.1016/j.msea.2014.01.024.

[18] Barbera D., Chen H., Liu Y., Creep-fatigue behaviour of aluminum alloy-based metal matrix composite. Int J Press Vessels Piping 2016;139-140:159-72. https://doi.org/10.1016/j.ijpvp.2016.02.004.

[19] Llorca J., Fatigue of particle- and whisker-reinforced metal-matrix composites. Prog Mater Sci 2002;47:283-353. https://doi.org/10.1016/S0079-6425(00)00006-2.

[20] Rojas JI., Venkata Siva B., Sahoo KL., Crespo D., Viscoelastic behavior of a novel aluminum metal matrix composite and comparison with pure aluminum, aluminum alloys, and a composite made of Al-Mg-Si alloy reinforced with SiC particles. J Alloys Compd 2018;744:445-52. https://doi.org/10.1016/j.jallcom.2018.02.103.

[21] Payten WM., Dean DW., Snowden KU., A strain energy density method for the prediction of creep-fatigue damage in high temperature components. Mater Sci Eng A 2010;527(7-8):1920-1925. https://doi.org/10.1016/j.msea.2009.11.028.

[22] Liao D., Zhu S-P., Gao J-W., Correia J., Calçada R., Lesiuk G., Generalized strain energy density-based fatigue indicator parameter. Int J Mech Sci 2023;254:108427. https://doi.org/10.1016/j.ijmecsci.2023.108427.

[23] Giuliano D., Barbera D., Chen H., Cho N-K., Liu Y., Creep-fatigue and cyclically enhanced creep mechanisms in aluminium based metal matrix composites. Eur J Mech A Solids 2019;74:66-80. https://doi.org/10.1016/j.euromechsol.2018.10.015.

[24] Paul SK., A critical review of experimental aspects in ratcheting fatigue: microstructure to specimen to component. J Mater Res Technol 2019;8:4894-914. https://doi.org/10.1016/j.jmrt.2019.06.014.

[25] Kan QH., Kang GZ., Zhang J., Uniaxial time-dependent ratchetting: visco-plastic model and finite element application. Theor Appl Fract Mech 2007;47:133-44. https://doi.org/10.1016/j.tafmec.2006.11.005.

[26] Mroziński S., Lis Z., Egner H., Energy dissipated in fatigue and creep conditions. Materials 2021;14:4724. https://doi.org/10.3390/ma14164724.

[27] Movaghghar A., Lvov GI., An energy model for fatigue life prediction of composite materials using continuum damage mechanics. Appl Mech Mater 2012;110:1353-1360. https://doi.org/10.4028/www.scientific.net/AMM.110-116.1353.

[28] Hiremath MM., Doshi N., Bernthaler T., Anger P., Mishra SK., Guha A., et al., 3D damage evolution and microstructural-based machine learning model for stiffness prediction in woven composite under cyclic loads. Int J Fatigue 2025;197:108913. https://doi.org/10.1016/j.ijfatigue.2025.108913.

[29] Wang Y., Huang M., Li Z., Void nucleation in heterogeneous materials induced by particle-matrix debonding in polycrystalline matrix. Eur J Mech A Solids 2026;116:105899. https://doi.org/10.1016/j.euromechsol.2025.105899.

[30] Prasad NE., Vogt D., Bidlingmaier T., Wanner A., Arzt E., Low cycle fatigue and creep-fatigue interaction in short fibre reinforced aluminium alloy composite. Mater Sci Technol 2010;26:1363-1372. https://doi.org/10.1179/026708309X12506933873620.

[31] Wang Y., Wang X., Yang Y., Lan X., Zhang Z., Li H., Study on creep-fatigue mechanical behavior and life prediction of Ti2AlNb-based alloy. Materials 2022;15(18):6238. https://doi.org/10.3390/ma15186238.

[32] Kindrachuk V., Fedelich B., Rehmer B., Peter F., Computational methods for lifetime prediction of metallic components under high-temperature fatigue. Metals 2019;9:390. https://doi.org/10.3390/met9040390.

[33] Miner MA., Cumulative damage in fatigue. J Appl Mech 1945;12(3):A159-164. https://doi.org/10.1115/1.4009458.

[34] Lemaitre J., A continuous damage mechanics model for ductile fracture. J Eng Mater Technol 1985;107(1):83-89. https://doi.org/10.1115/1.3225775.

[35] Chaboche JL., Continuum damage mechanics: part I — general concepts. J Appl Mech 1988;55:59-64. https://doi.org/10.1115/1.3173661.

[36] Shen M-HH., Akanda SR., A modified closed form energy-based framework for fatigue life assessment for aluminum 6061-T6: strain range approach. Int J Damage Mech 2016;25:661-71. https://doi.org/10.1177/1056789516635726.

[37] Kaleva O., Orelma H., Petukhov D., Parameter estimation of a high-cycle fatigue model combining the Ottosen-Stenström-Ristinmaa approach and Lemaitre-Chaboche damage rule. Int J Fatigue 2021;147:106153. https://doi.org/10.1016/j.ijfatigue.2021.106153.

[38] Lukichev A., Physical meaning of the stretched exponential Kohlrausch function. Phys Lett A 2019;383(25):2983-2987. https://doi.org/10.1016/j.physleta.2019.06.029.